Integrated clinical, whole-genome, and transcriptome analysis of multisampled lethal metastatic prostate cancer

G. Steven Bova,[1,3] Heini M.L. Kallio,[1,3] Matti Annala,[1,3] Kati Kivinummi,[1] Gunilla Högnäs,[1] Sergei Häyrynen,[1] Tommi Rantapero,[1] Virpi Kivinen,[1] William B. Isaacs,[2] Teemu Tolonen,[1] Matti Nykter,[1] and Tapio Visakorpi[1]

[1]Prostate Cancer Research Center, Institute of Biosciences and Medical Technology, BioMediTech, University of Tampere and Fimlab Laboratories, Tampere University Hospital, FI-33014 Tampere, Finland; [2]The James Buchanan Brady Urological Institute, Johns Hopkins University School of Medicine, Baltimore, Maryland 21287, USA

Abstract We report the first combined analysis of whole-genome sequence, detailed clinical history, and transcriptome sequence of multiple prostate cancer metastases in a single patient (A21). Whole-genome and transcriptome sequence was obtained from nine anatomically separate metastases, and targeted DNA sequencing was performed in cancerous and noncancerous foci within the primary tumor specimen removed 5 yr before death. Transcriptome analysis revealed increased expression of androgen receptor (AR)-regulated genes in liver metastases that harbored an *AR* p.L702H mutation, suggesting a dominant effect by the mutation despite being present in only one of an estimated 16 copies per cell. The metastases harbored several alterations to the PI3K/ AKT pathway, including a clonal truncal mutation in *PIK3CG* and present in all metastatic sites studied. The list of truncal genomic alterations shared by all metastases included homozygous deletion of *TP53*, hemizygous deletion of *RB1* and *CHD1*, and amplification of *FGFR1*. If the patient were treated today, given this knowledge, the use of second-generation androgen-directed therapies, cessation of glucocorticoid administration, and therapeutic inhibition of the PI3K/AKT pathway or FGFR1 receptor could provide personalized benefit. Three previously unreported truncal clonal missense mutations (*ABCC4* p.R891L, *ALDH9A1* p.W89R, and *ASNA1* p.P75R) were expressed at the RNA level and assessed as druggable. The truncal status of mutations may be critical for effective actionability and merit further study. Our findings suggest that a large set of deeply analyzed cases could serve as a powerful guide to more effective prostate cancer basic science and personalized cancer medicine clinical trials.

[Supplemental material is available for this article.]

INTRODUCTION

Although whole-genome sequencing (WGS) has been reported from roughly 2500 individual human cancer primary tumors to date (Ding et al. 2010, 2014; Bass et al. 2011; Berger et al. 2011, 2012; Chapman et al. 2011; Roychowdhury et al. 2011; Ellis et al. 2012; Egan

Corresponding author: tapio.visakorpi@uta.fi

[3]These authors contributed equally to this work.

et al. 2012; Govindan et al. 2012; Imielinski et al. 2012; Nik-Zainal et al. 2012; Turajlic et al. 2012; Walter et al. 2012; Welch et al. 2012; Baca et al. 2013; Beà et al. 2013; Brastianos et al. 2013; Brennan et al. 2013; Dulak et al. 2013; Ho et al. 2013; Kan et al. 2013; Morin et al. 2013; Newburger et al. 2013; Pugh et al. 2013; Zhang et al. 2013; Bruin et al. 2014; Chen et al. 2014, 2015; Morrison et al. 2014; Nadauld et al. 2014; Ouyang et al. 2014; Wang et al. 2014; Andersson et al. 2015; Engle et al. 2015; Cooper et al. 2015; Kovac et al. 2015; Kim et al. 2015; Yates et al. 2015), only a small number of studies have compared WGS data from multiple metastatic tumors and primary tumors from the same individual (Gundem et al. 2015; Hong et al. 2015; Patch et al. 2015). The recent WGS study of multiple prostate cancer metastases and primary tumor samples from 10 individuals (Gundem et al. 2015) allows comparison of the research value of WGS studies confined to dozens or hundreds of samples of primary tumors ("wide" studies) versus studies that include both primary and multiple metastases ("deep" studies). "Wide" studies have begun to establish the landscape of mutations typical for a given cancer and cohort of patients, whereas "deep" studies allow phylogenetic tracing and analysis of features of tumor clonality and evolution in response to therapy and linked to the metastatic phenotype, features that arguably have greater implications for the development of effective precision treatment of cancer than the cataloging of common mutations.

Combined analysis of primary and metastatic samples from individual prostate cancer patients is particularly important in light of recent reports showing that lethal metastatic cancers can arise from low Gleason grade primary cancer foci in the context of higher Gleason grade foci in the same patient (Haffner et al. 2013) and that even extensive needle biopsies may miss the focus of tumor that gives rise to lethal disease (Haffner et al. 2015; Lindberg et al. 2015).

Here we report the first combined analysis of transcriptome sequence, detailed clinical history, and whole-genome sequencing of primary tumor sites and multiple metastases from a single patient (A21), deepening the analysis of this case beyond the WGS data already reported in Gundem et al. (2015), and report our findings from the point of view of personalized cancer medicine.

RESULTS

Clinical Presentation and Family History

Initial clinical concern was raised when the patient (A21) was found to have elevated serum prostate-specific antigen (PSA) (25.2 ng/mL) at the age of 65 (Fig. 1A). Prostate digital rectal examination after the PSA test results were available showed a "large fleshy prostate, approximately 45–60 grams, with subtle induration located deep within the right base of the gland. The margins were normal." Transrectal ultrasound showed "cysts and calcifications in the central zone compatible with benign prostatic hyperplasia, as well as hypoechoic nodules in the peripheral zone in the midline, on the right and the left, which were suspicious for malignancy. The prostate capsule appeared intact and the seminal vesicles appeared normal." Prostate biopsy contained adenocarcinoma Gleason score 4 + 3 = 7. Family history was negative for prostate cancer. A21's mother died of breast cancer in her 80s. Bone scan performed 50 d after biopsy diagnosis was suspicious for bone metastasis; follow-up radiographs showed degenerative disk disease, mild osteoporosis, a possible healed rib fracture, and "no definitive evidence of metastatic foci." Radical prostatectomy 3 mo after prostate biopsy contained Gleason 4 + 3 = 7 adenocarcinoma with a minor component of Gleason grade 5 carcinoma. The right posterior aspect of the prostate contained established capsular penetration and surgical margin positive for adenocarcinoma. Seminal vesicles, five right pelvic lymph nodes, and seven left pelvic lymph nodes were negative for tumor.
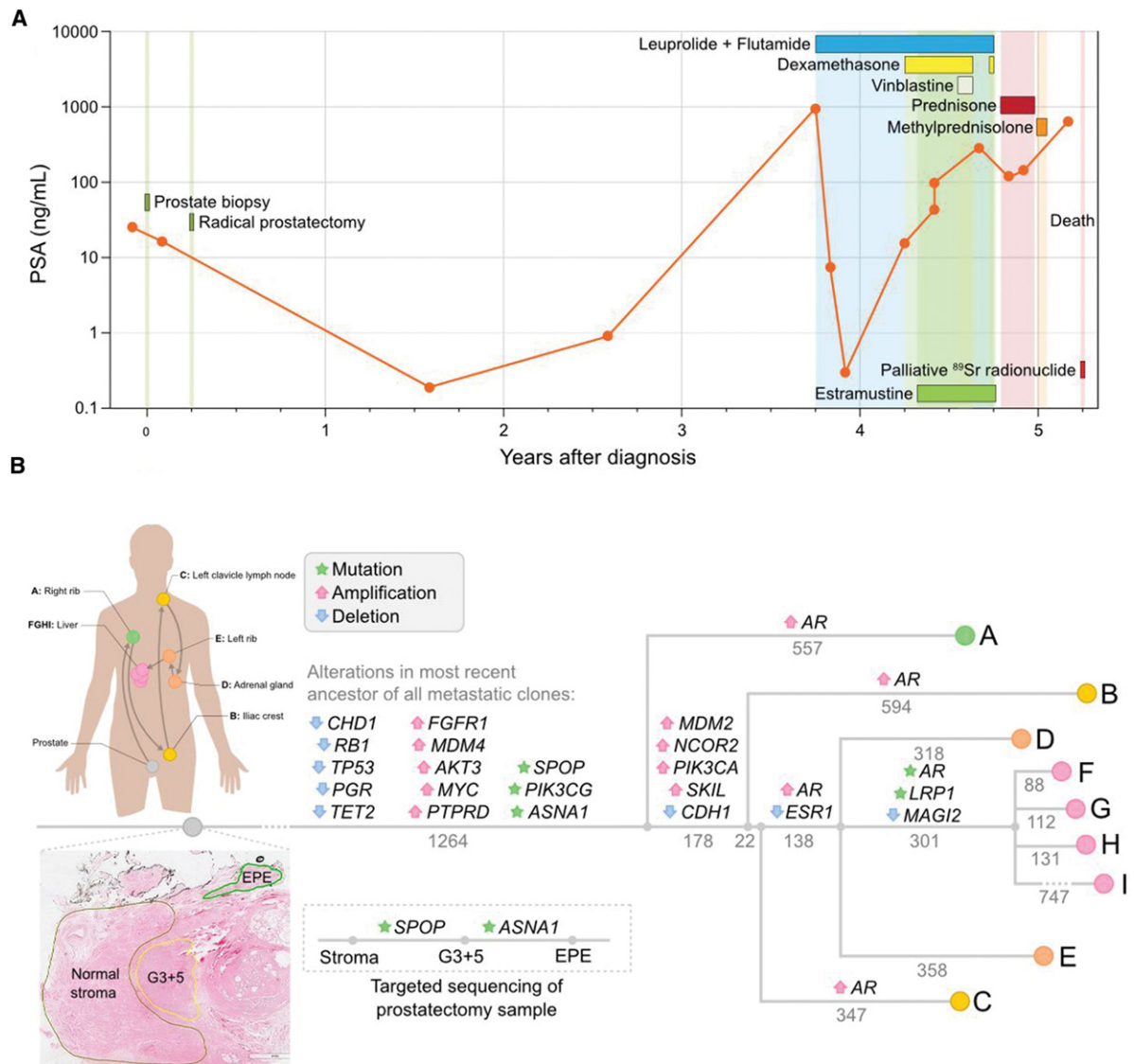
Figure 1. Case A21 clinical timeline and pathology-genomic relationships. (*A*) Clinical events and serum PSA plotted with time in years on *x*-axis. (*B*) Three regions of radical prostatectomy tissue were microdissected (normal stroma, a mixed Gleason 3 + Gleason 5 cancer region, and a region of extraprostatic extension containing Gleason grade 5 cancer) and compared by targeted sequencing to whole-genome sequence data from nine metastatic sites. Mutation patterns show that the two primary cancer sites and nine metastatic sites are part of a clonal cancer lineage, as reflected by accretion of mutations in *SPOP*, *ASNA1*, and *PIK3CG* and others. The mixed Gleason 3 and Gleason 5 primary cancer region contains the earliest common ancestor identified, and cancer cells in the region of extraprostatic extension are more closely related to cells in all metastatic sites studied. All metastatic sites contain a *PIK3CG* p. R472 missense mutation that was not identified in the primary cancer. The pattern of spread of the metastatic tumor implied from the genomic data is shown. Numbers of unique high-confidence somatic mutations identified in metastases are listed in gray and horizontal lines are proportional in length to mutation number, with 1264 mutations shared by all metastases, an additional 557 somatic mutations unique to A, 178 mutations shared by all other metastases, and so forth. G, Gleason grade; EPE, extraprostatic extension; LN, lymph node.

Serum PSA was <0.2 ng/mL, 1.6 yr after initial biopsy diagnosis. Of note, 3.8 yr after prostatectomy, the patient developed bone pain, his PSA elevated to 969 ng/mL, and a bone scan showed diffuse skeletal metastases. A luteinizing hormone-releasing hormone (LHRH) analog, leuprolide, combined with an antiandrogen, flutamide, was started. Serum PSA dropped to 0.2 ng/mL and then rose again to 15.8 ng/mL. This was accompanied by reoccurrence of bone pain 6 mo after beginning leuprolide plus flutamide, at which point the patient began treatment with a series of corticosteroids (Fig. 1A), as well as estramustine and vinblastine. Vinblastine treatment was associated with transient decrease in PSA. Of note, 225 d before death, flutamide and leuprolide were stopped according to available records. The patient developed severe bone pain poorly controlled with opioid and other pain medications, and he elected to undergo intravenous ^{89}Sr radionuclide treatment 46 d before death from metastatic prostate cancer. The last measured serum PSA level 64 d before death was 643.1 ng/mL. The age at prostate biopsy diagnosis of prostate cancer for subject A21 has been shifted by a randomly selected number between −3 and +3 yr in accordance with study subject's consent to participate. Clinical values have also been altered to reduce the risk of reidentification of the subject without altering clinical meaning.

Patient A21 was treated in the 1990s. All of the available PSA, chemotherapy, steroid therapy, and radiotherapy data for the patient are shown. A21 was not considered for adjuvant radiotherapy after radical prostatectomy, for unclear reasons. A21 appears to have avoided returning to his physician after the PSA initially rose to 0.9 ng/mL, after radical prostatectomy, until he developed severe pain. It is also not clear from the available records why leuprolide and flutamide were stopped 225 d prior to death, when he was transferred to a long-term care facility. We speculate that since A21's prostate cancer was progressing despite androgen deprivation therapy (ADT) using leuprolide and flutamide, his clinicians felt it was no longer needed.

Whole-Genome Sequencing

We performed whole-genome sequencing (WGS) in nine and whole-transcriptome sequencing (RNA-seq) in six of the same metastatic cancer samples obtained in a rapid autopsy study.

Phylogenetic Analysis

Analysis of somatic mutations across metastases revealed the order of clonal evolution from right rib nodular metastasis through several intermediate locations to four liver sites in the final stages of the disease (Fig. 1B). This was confirmed by analysis of DNA rearrangements and somatic copy-number alterations (Supplemental Figs. 1 and 2). The chain-like rearrangements suggestive of chromoplexy present only in these liver metastases demonstrate that major genome crisis events continue to occur during cancer progression (Baca et al. 2013).

All metastases showed amplification of the androgen receptor (*AR*) locus (Fig. 2A). *AR* locus instability was characterized by four distinct patterns suggesting that *AR* instability arose independently in the four earliest metastatic sites, consistent with sudden strong selection pressure to maintain androgen signaling after onset of ADT (Palmberg et al. 2000) (see Methods). We additionally found evidence for a late-stage *AR* p.L702H missense mutation in all four liver metastases (Table 1). The mutant allele fraction indicated a single mutant copy of *AR* in the setting of ~16-fold *AR* amplification (Fig. 2B). The left adrenal metastasis also yielded a single p.L702H read, but sequencing error could not be ruled out (Fig. 2B). None of the metastases showed evidence of significant expression of *AR* cryptic exon variants.

Transcriptome Sequencing

RNA-seq in the six metastatic sites demonstrated significant up-regulation of androgen-regulated genes in samples with the *AR* p.L702H mutation (Fig. 2C). The p.L702H mutant is
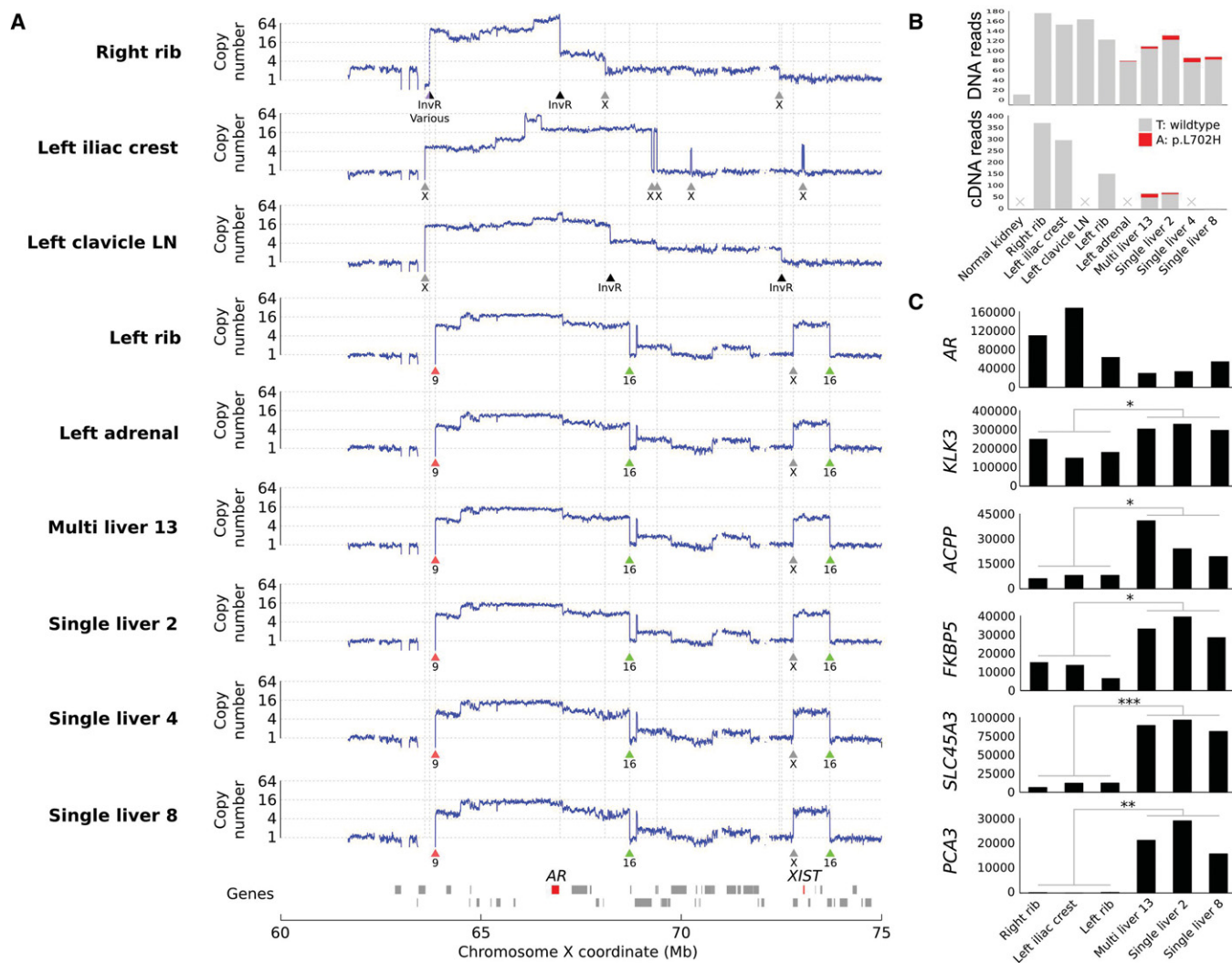
Figure 2. Evolution of androgen receptor (*AR*) region X Chromosome alterations by whole-genome and transcriptome sequencing in case A21. (*A*) *AR* regional structural instability signature in earlier metastases (right rib, left iliac crest, left clavicle LN, and left adrenal) in the clonal evolution map shown in Figure 1B contain four distinct patterns, the latter of which (left adrenal) is shared by all subsequent sites on the map, suggesting independent evolutionary selection of distinct *AR* structural response to androgen deprivation therapy (ADT) in at least these four studied independent sites. Whether these assorted *AR*-mutated subclones existed in small numbers before selection cannot be determined from the current study. (*B*) All four liver metastases and the left adrenal metastasis contained an *AR* p.L702H mutation in one copy of *AR*. The mutation is also present in the RNA-seq data from the same samples. The L702H mutant modifies the AR ligand binding domain and is known to alter ligand specificity, rendering the protein responsive to glucocorticoids administered during A21's treatment shown in Figure 1A (Zhao et al. 2000; Carreira et al. 2014). (*C*) Liver metastases containing the *AR* p.L702H mutation exhibited significantly increased expression of androgen-regulated genes *KLK3*, *ACPP*, *FKBP5*, *SLC45A3*, and *PCA3* as compared with three metastatic sites where the *AR* p.L702H was not detected (*$P < 0.05$, **$P < 0.01$ and ***$P < 0.001$; see Methods).

known to have increased affinity for glucocorticoids leading to AR transactivation (Zhao et al. 2000; Carreira et al. 2014). If a patient with similar findings were alive today, detection of mutant AR might indicate halting corticosteroid treatment, with potential benefit to the patient. The findings indicate that the *AR* locus can be targeted by two hits (*AR* amplification and

Table 1. Selected missense variants based on whole-genome sequencing

						Number of variant reads/total reads									
Chr	Position	Ref	Alt	Gene	AA_Change	Normal kidney	Right rib	Left iliac crest	Left clavicle LN	Left adrenal	Left rib	Single liver 4	Single liver 8	Single liver 2	Multi liver 13
Chr3	178936094	C	A	*PIK3CA*	p.Q546K	0/33	0/32	0/56	0/33	0/60	18/59	0/48	0/66	0/54	0/37
Chr1	165664551	A	G	*ALDH9A1*	p.W89R	0/29	18/29	17/27	16/24	23/37	26/36	22/32	18/29	19/26	21/29
Chr7	106509420	C	T	*PIK3CG*	p.R472C	0/35	7/25	11/36	12/42	8/24	12/38	8/19	8/24	7/47	15/38
Chr13	95735408	C	A	*ABCC4*	p.R891L	0/30	13/24	25/44	25/31	16/26	20/35	20/32	18/27	22/33	15/28
Chr17	47696643	A	C	*SPOP*	p.F102C	0/35	16/22	7/25	6/18	8/24	14/34	12/20	12/26	16/32	16/29
Chr19	12849387	C	G	*ASNA1*	p.P75R	0/33	8/16	13/29	15/30	6/20	9/25	9/19	10/19	16/38	14/33
ChrX	66931463	T	A	*AR*	p.L702H	0/19	0/176	0/153	0/164	1/83	0/127	8/132	8/91	5/94	4/112

Ref, A21 germline reference allele; Alt, A21 alternative allele; AA_Change, predicted protein amino acid change.

mutation), underscoring the importance of androgen signaling in prostate cancer progression. All of the patient's sequenced metastases were negative for ETS (E26 transformation specific) fusions.

Targeted Sequencing

To trace the origin of the alterations found in the metastases, we performed targeted sequencing of three foci in the prostate: a region containing mixed Gleason grade 3 and 5 cancer, a region of extraprostatic extension (EPE) containing Gleason grade 5 cancer, and a region of noncancerous prostate stroma (Fig. 1B). Based on sequence analysis of these foci, the metastases most closely match mutations found in the region of EPE. Both the region of mixed Gleason 3 and Gleason 5 cancer and the region of Gleason 5 EPE contain a *SPOP* p.F102C mutation (Barbieri et al. 2012).

DISCUSSION

Examining the findings in the metastases at the *AR* locus together with the clinical timeline, we speculate that metastatic prostate cancer subpopulation selection occurred in three phases. Phase 1 occurred at the time of initial ADT, when four independent *AR*-amplified subclones emerged in four separate locations (Figs. 1A and 2A). Phase 2 is indicated by the emergence of an *AR* p.L702H mutation conferring glucocorticoid responsiveness (Figs. 1A, 2B,C). Phase 3 occurred when leuprolide and flutamide treatment were stopped 225 d before death, when the most highly androgen-plus-corticosteroid responsive subclone rapidly emerged and populated the liver (Figs. 1A, 2B).

Shared truncal driver mutations in metastases are attractive potential targets for personalized therapy. In A21, we found six potentially actionable genomic alterations shared by all metastases and expressed at the RNA level, including four point mutations and two copy-number alterations (Supplemental Table 1). The PI3K/AKT pathway harbored several potentially activating alterations, including an *AKT3* duplication and *PIK3CG* p.R472C mutation in all metastases, and a *PIK3CA* duplication in all metastases except the right rib metastasis. The left rib metastasis additionally harbored a private *PIK3CA* p.Q546K mutation (Table 1). Mutations at this residue disrupt the PI3KCA helical domain and are known to result in PI3K pathway activation. PIK3CA encodes a catalytic subunit of the class IA phosphoinositol-3-kinase (PI3K) complex, whereas PIK3CG encodes a catalytic subunit of the class IB

PI3K complex. Both class I PI3K complexes phosphorylate PIP_2 lipids to produce PIP_3. PIP_3 lipids bind to the plasma membrane and provide a docking point for AKT family proteins (including AKT3) and their upstream activator PDK1, resulting in activated AKT signaling. Although the biological significance of the *PIK3CG* p.R472C mutation is unclear, the multiple hits to this pathway suggest that the patient could have benefited from PI3K/AKT pathway inhibition through drugs such as NVP-BEZ235 or AZD5363. Another potentially actionable finding was a focal *FGFR1* amplification shared by all metastases. Aberrant activation of fibroblast growth factor receptors by amplification or fusion has been associated with oncogenic progression in various cancers including prostate cancer (Armstrong et al. 2011), and FGFR1 inhibitors are currently being tested in clinical trials (Dieci et al. 2013).

Three of A21's clonal truncal mutations (*ABCC4* p.R891L, *ALDH9A1* p.W89R, and *ASNA1* p.P75R) (Table 1; Supplemental Table 1) were expressed at the RNA level and were assessed as potentially druggable based on analysis using the Drug–Gene Interaction Database (Griffith et al. 2013). Although these truncal mutations likely represent passenger events, they could introduce physiologic vulnerabilities for small-molecule-based synthetic lethality and/or create novel targets for immunotherapy. Expressed clonal truncal mutations that fall into this "potentially helpful passenger" category merit further analysis to determine their true value in advancing cancer precision medicine.

What added value did WGS provide in this study? Would whole-exome sequencing (WES) have provided similar information? WGS was critical for understanding the clonal history of the metastases, as WES would have reduced the number of informative mutations from 741 to below 20. This number of mutations would not have been sufficient for reconstructing the clonal history with high confidence. Use of exome sequencing would have also rendered detailed analysis of the *AR* copy-number alterations and their breakpoints impossible. These are research findings with potential clinical import, supporting the further use of WGS in appropriate trials. Nonetheless, using the WGS data to simulate WES in each metastasis studied in this case shows that 35–43 protein-altering mutations would have been identified, 32 of which were shared by all metastases (including the four potentially druggable protein-altering mutations in *PIK3CG*, *ABCC4*, *ALDH9A1*, and *ASNA1*). A matrix of protein-altering mutations shared by any two metastases shows that the 32 truncal mutations could be perfectly or nearly perfectly separated from the nontruncal mutations by combining results of any two bone metastasis samples or combination of one bone and one visceral metastasis samples. This finding should be tested in future studies (Table 1; Supplemental Table 3).

How does this case compare to the cases in the recent clinical exome sequencing in advanced prostate cancer study with 150 patients (Robinson et al. 2015)? Based on Figure 2 in Robinson et al., Case A21 reported here has interesting similarities to Case 32 in Robinson et al. These two cases share *AR* amplification and loss of both copies of *TP53*; neither has loss of *PTEN* or contains *ETS* fusions; A21 has missense mutations in one copy of PI3 kinase core protein *PIK3CG*; Case 32 has amplification of both copies of PI3 kinase core protein *PIK3CB*; both cases show loss of *CHD1* (both copies in Case 32, hemizygous in Case A21); and both have missense mutation of one copy of *SPOP*. Genomic differences include alterations in *BRCA2* in Case 32 only, and loss of *RB1* and *TET2* in A21 only. *FGFR1* is amplified in A21, and none is reported for Case 32. Whether these similarities and differences are meaningful on a biologic or clinical level would require more detailed comparison using well-curated databases and a larger number of cases, but they suggest that the field would likely benefit from the ability to do such comparisons. In conclusion, analysis of the "deep" data set available for Case A21 provides biological insights relevant to prostate cancer biology in general and to Case A21 in particular. These insights are far more useful than what can typically be obtained from "wide" studies.

In conclusion, this case study suggests that once initial selection of castration-resistant subclones occurs after initial ADT, androgen responsiveness is nonetheless maintained by

metastatic cells. Reintroduction of androgen by stopping leuprolide and flutamide and continuing corticosteroids was associated with population of the liver by a clone containing combined amplified wild-type and corticosteroid-sensitive mutant AR. In addition, p.L702H AR mutation in approximately one of 16 *AR* copies per cell was associated with activation of androgen-responsive elements as evidenced by RNA-seq. Importantly, this study adds to previous reports questioning the validity of molecular representation provided by random biopsies of the primary tumor. To find the best potential novel drug targets for individual patients, studies are needed to determine optimal sampling regimes, including "liquid" and metastatic tissue biopsies at different time points, to identify truncal changes, and to detect therapy-induced changes. Studies fully integrating the entire clinical timeline, pathology, and genomic findings in individual patients are essential for meaningful progress in understanding cancer and can teach the combined research and medical team to identify potentially actionable alterations. We argue that such "deep" studies should become the rule, rather than the exception. Finally, identification of novel "precision" druggable targets is just a first step. Currently many patients are not eligible to receive identified targeted drugs because of limitations in trial and reimbursement mechanisms. New clinical trial and drug approval and reimbursement mechanisms are needed to allow the cancer precision medicine concept to find its appropriate use in medical practice.

METHODS

Tissue Microdissection and DNA Isolation

DNA and RNA isolation from the freshly frozen cryostat-microdissected metastases (*n* = 9; Fig. 3B) was performed with phenol–chloroform extraction or QIAGEN column extraction. A noncancerous kidney sample was used as germline reference control. Cancer cell fraction (CCF) estimated by visual analysis of hematoxylin and eosin–stained dissected tumor sections and from examination of allelic fractions was between 75% and 90% (mean CCF was 84.6%) for all tumor samples. WGS was performed for all nine metastatic samples and RNA-seq was performed in six of the same metastatic tissue materials (alternating sections used for DNA or RNA isolation). Laser microdissection of selected foci (Fig. 1B) from the prostate removed 5 yr before death was performed using Arcturus and MMI dissection systems. DNA isolation was performed using QIAGEN FFPE kits.

Whole-Genome Library Construction and Sequencing

Genomic DNA was sheared into 500-bp fragments using a Covaris E210 ultrasonicator. Overhangs were converted into blunt ends using T4 DNA polymerase and Klenow enzyme. An adenine was added to the 3′ end of the blunt phosphorylated DNA fragments, and adapters were ligated on both ends. Ligated products were purified by agarose gel electrophoresis followed by QIAquick gel extraction, to remove residual free and self-ligated adapters and to select properly sized templates for cluster generation. DNA fragments with adapters on both ends were amplified using two primers that annealed to the adapters. Polymerase chain reaction (PCR) products were checked and purified by agarose gel electrophoresis. The fragment size and molar concentration of each library were determined using the Agilent 2100 Bioanalyzer and ABI Real-Time PCR System (StepOnePlus), respectively. As mean fragment size increased to 622 bp after adapter ligation, fragments between 600 bp and 684 bp were selected. An Illumina Cluster Station was used to hybridize samples onto a flow cell and amplify them for sequencing on Illumina HiSeq 2000. Raw image files were processed by Illumina pipeline for base-calling with default parameters resulting in 90-bp paired-end reads. Reads with too many N bases (>10%) or low base quality (>50%

Table 2. The coverage of the whole-genome and whole-transcriptome sequencing

Sample	Whole-genome sequencing			Whole-transcriptome sequencing		
	Total reads	Aligned (%)	Median CDS coverage	Total reads	Aligned (%)	mtRNA (%)
Right rib	1,200,343,314	93	26	108,387,928	68	15
Left iliac crest	1,379,274,636	94	37	105,250,920	55	10
Left clavicle LN	1,126,637,546	93	31	110,086,613	91	82
Left adrenal	1,151,593,908	93	27			
Left rib	1,252,845,806	93	30	110,678,869	73	8
Single liver 2	1,481,140,684	91	38	108,970,487	93	9
Single liver 4	1,077,269,004	92	23			
Single liver 8	1,164,407,226	92	24	11,237,2452	88	12
Multi liver 13	1,088,762,606	92	28	113,997,841	93	10
Normal kidney	1,169,821,684	91	34			

CDS, coding DNA sequence; mtRNA, mitochondrial RNA.

bases with base quality <5) were discarded. Library construction and sequencing was performed at BGI (Hong Kong). Average whole-genome sequence coverage was 30× for cancerous and noncancerous samples. Median coverage of coding regions was 23× or higher in all samples (Table 2). The range of coverage at different depths for each tumor sample is shown in Supplemental Figure 4.

Targeted Sequencing

To validate mutations found by whole-genome sequencing and to sequence microdissected regions from the primary tumor, targeted sequencing of 88 amplicons (average 150 bp in length) was carried out using Illumina MiSeq and an Illumina TruSeq Custom Amplicon kit designed using Illumina Design Studio software. Of the 88 amplicons, 63 amplicons were targeted at somatic mutations, five targeted at germline single-nucleotide polymorphisms (SNPs) were used as positive controls, and the remaining 20 were used for assessing copy number.

The list of 63 somatic mutation targets included 17 protein-altering mutations observed in all metastases, 16 protein-altering mutations observed in a subset of metastases, and 30 non-CDS (coding sequence) mutations that were validated because they were informative with regard to the progression model (Supplemental Table 2). Of the 63 targeted mutations, 60 yielded reads, and 57 of 60 (95%) yielded genotype calls identical to those obtained from whole-genome sequencing. Three targeted mutations yielded low mutant allele fraction in all samples (including the normal tissue) and were recategorized as sequencing errors.

Amplicons used for copy-number assessment included five amplicons each for *TP53*, *RB1*, *CHD1*, and the 23-Mb region in Chromosome 2. These four regions were deleted in all metastases, and the amplicons were included to assess their copy number in the prostatectomy sample.

Whole-Transcriptome Library Construction and Sequencing

RNA isolated from seven of the metastases underwent transcriptome sequencing. Beads with oligo(dT) were used to isolate poly(A) mRNA after collection of total RNA. Fragmentation buffer was added to shear mRNA into short fragments and to synthesize the first-strand cDNA with random hexamer primers. The second-strand cDNA was synthesized using buffer, dNTPs, RNaseH, and DNA polymerase I, respectively. Short fragments

were purified with the QIAquick PCR Extraction Kit and resolved with elution buffer (EB) for end reparation and poly(A) addition. After that, the short fragments were ligated to sequencing adapters and suitable fragments were selected for the PCR amplification as templates and separated with agarose gel electrophoresis before sequencing. Raw image files were processed by Illumina Pipeline for base-calling with default parameters resulting in 90-bp paired-end reads. Reads with too many N bases (>10%) or low base quality (>50% bases with base quality <5) were discarded. Library construction and sequencing was performed at BGI, Hong Kong. One transcriptome sample 80% contaminated with mitochondrial RNA (mtRNA) was eliminated from analysis, resulting in six samples with good quality sequence.

Mutation Analysis

Whole-genome sequencing reads were aligned against the GRCh37 human reference genome using Bowtie version 2.0.0 (Langmead and Salzberg 2012). Duplicate alignments were removed using SAMtools rmdup. A somatic mutation was called in a tumor sample if at least four reads and at least 15% of all reads displayed the mutant allele, and if at most one read and at most 5% of all reads in the normal kidney sample displayed the same allele. Pearson's χ^2 test was additionally used to assess the probability that all samples (including the normal sample) had the same underlying allele fraction (indicating a sequencing error). Mutations with a *P*-value > 0.0001 were discarded. Finally, mutations at sites annotated in the 1000 Genomes database (The 1000 Genomes Project Consortium 2015) with a minor allele fraction above 0.5% were discarded. The ANNOVAR toolkit (Wang et al. 2010) was used to annotate the genomic locations and predicted consequences of somatic mutations.

Putative Druggable Targets

To identify putative druggable targets, a list of genes with nonsynonymous variants in coding regions and genes with focal high-level amplification was queried against DGIdb version 1.66 (Griffith et al. 2013).

Identification of Chromosomal Rearrangements

Chromosomal rearrangements were called using the Breakfast algorithm, part of the Pypette suite (https://github.com/annalam/pypette). Briefly, the software looks for paired-end reads and individual mates overlapping a chromosomal breakpoint and identifies high-confidence rearrangements at sites with multiple reads of evidence. Minimum evidence was two paired-end reads and two individual mates spanning the junction. The normal kidney sample was used as control to determine somatic rearrangements.

Transcriptome Analysis

The paired-end 90-bp reads from HiSeq 2000 sequencing were aligned against the GRCh37 reference genome and National Center for Biotechnology Information (NCBI) transcriptome annotations using TopHat 2.0.6. The alignment statistics of the samples are given in Table 1. The number of reads aligned to the exons of Ensembl 68 genes were counted using BEDTools (Quinlan and Hall 2010). Read counts were normalized across samples using median-of-ratios normalization.

Progression Model

To infer the clonal history of metastases in patient A21, we first constructed a mutation matrix containing all 741 high-confidence somatic mutations found in exactly two to eight metastases. Mutations found in all metastases or mutations found in only one metastasis provided no information for clonal inference and were omitted from analysis. Hierarchical clustering of

the mutation matrix revealed linear accumulation of somatic mutations as new metastases were seeded from a truncal clone (Supplemental Fig. 3). The most recent common ancestral clone (MRCAC) of all metastases had acquired 1264 somatic mutations by the time of metastatic seeding to the right rib (not shown in the matrix). The MRCAC then acquired 178 additional mutations before seeding to the left iliac crest and a further 22 mutations before seeding to the left clavicle. The clonal history was inferred by considering triplets of metastases. If we denote three arbitrary metastases as A, B, and C, we inferred that metastases B and C occurred later than metastasis A and shared an ancestral clone with A if (1) metastases B and C shared a significant number of mutations not present in A; (2) all mutations shared by A and B were present in C; and (3) all mutations shared by A and C were present in B. We cannot require that all mutations in A should also be present in later metastases B and C, because metastasis A will generally have acquired private mutations not present in the MRCAC of A, B, and C.

Because the mutation matrix only displays mutations shared by two or more metastases, private mutations are not visible and therefore we observe a clear visual pattern whereby later metastases carry all of the nonprivate mutations found in earlier metastases (in the absence of branched evolution).

One interesting outcome of the mutation matrix visualization is that it makes it clear how copy-number alterations can confound analyses of clonal history. In the mutation matrix for Patient A21, many mutations observed in the right rib metastasis were lost in later metastases because of deletion events in Chromosomes 2, 6, 7, and 11 (Supplemental Fig. 3). Whole chromosome deletion of Chromosome 11 occurred as two independent events: once as a private event in the left clavicle lymph node metastasis, and a second time in MRCAC of the left rib metastasis and subsequent metastases. In total, 654 of 741 (88.2%) somatic mutations were in perfect agreement with the proposed progression model. Of the 87 mutations that disagreed with the model, 80 were explained by copy-number alterations that deleted the mutant allele or diluted the mutant allele fraction.

It should be noted that the sequencing data alone is not sufficient for making inferences about the physical location of the truncal clone from which metastases were seeded. It is possible that all metastases were seeded from the right rib metastasis or from a different metastatic site that was not sequenced or no longer existed at the time of autopsy. It is also possible that the site from which metastatic seeding occurred changed its location as the disease progressed.

The mutation matrix allows a reader to visually verify the inferred clonal history and clearly shows the confounding effect of copy-number alterations on clonal inference.

AR Amplification Analysis

We observed four distinct patterns of *AR* amplification among the nine metastases sequenced in this study and hypothesized that these *AR* amplifications arose independently in four metastases after ADT initiation. The alternate hypothesis was that the *AR* amplification arose in a single metastasis and underwent incremental evolution in clonal descendants to form the four observed structures. We find that independent evolution is the preferred hypothesis based on the following observations.

1. A bone scan performed just before starting ADT revealed multiple diffuse skeletal metastases, suggesting that independent evolution of *AR* amplifications in spatially disjoint metastases was possible.

2. No breakpoints were shared by the four distinct *AR* amplification structures. If incremental evolution of the *AR* locus had taken place, numerous shared breakpoints would be expected.

3. The structure of the *AR* locus only differed in the first four metastases. The last six metastases all shared an identical structure of the *AR* locus. If we assume that incremental evolution did take place in the first four metastases, why did it cease for the last six metastases?

AR Target Gene Analysis

In six A21 metastatic samples where analyzable transcriptome data were available, AR target transcript copy was significantly higher in three metastases containing the *AR* p.L702H mutation (Multi Liver 12, Single Liver 2, Single Liver 8) as compared with three metastatic sites not containing the *AR* p.L702H mutation (right rib, left iliac crest, left rib). These differences are statistically significant by two-tailed *t*-test with the following *P*-values: *KLK3* (0.0199), *ACPP* (0.0344), *FKBP5* (0.0344), *SLC45A3* (0.000078), and *PCA3* (0.0048) (Fig. 2C).

ADDITIONAL INFORMATION

Ethics Statement

Patients with metastatic prostate cancer provided written informed consent to participate in an integrated clinical–molecular study of metastatic prostate cancer (PELICAN), which was approved by the Johns Hopkins Medicine Institutional Review Board. A protocol, including collection and curation of medical records, survey, and tissue curation, was performed, including a special autopsy procedure designed to enable genomic tracing. Of 33 men who underwent autopsy as part of the study, A21 was selected for pilot integrative genome analysis because of the large number of metastases and primary cancer material available for study.

Data Deposition and Access

Whole-genome, targeted sequencing, and RNA-seq data have been deposited at the European Genome-phenome Archive (EGA; https://www.ebi.ac.uk/ega/) under accession numbers EGAS00001000262 and EGAS00001001659. The interpreted variants have been deposited in ClinVar (http://www.ncbi.nlm.nih.gov/clinvar/) under accession numbers SCV000259002–SCV000259062.

Acknowledgments

Author Contributions

The study was designed by G.S.B, T.V., and M.N. Data was collected by G.S.B., H.M.L.K., K.K., and G.H. Clinical data analysis was performed by G.S.B, H.M.L.K., and G.H. Pathology data analysis was performed by G.S.B. and T.T. Bioinformatic data analysis was performed by M.A., S.H., T.R., V.K., and M.N. Figures were generated by M.A., G.S.B., and M.N. The manuscript was written by G.S.B. and edited by T.V., M.N., M.A., W.B.I, and H.M.L.K.

REFERENCES

Andersson AK, Ma J, Wang J, Chen X, Gedman AL, Dang J, Nakitandwe J, Holmfeldt L, Parker M, Easton J, et al. 2015. The landscape of somatic mutations in infant MLL-rearranged acute lymphoblastic leukemias. *Nat Genet* **47:** 330–337.

Armstrong K, Ahmad I, Kalna G, Tan SS, Edwards J, Robson CN, Leung HY. 2011. Upregulated FGFR1 expression is associated with the transition of hormone-naive to castrate-resistant prostate cancer. *Br J Cancer* **105:** 1362–1369.

Baca SC, Prandi D, Lawrence MS, Mosquera JM, Romanel A, Drier Y, Park K, Kitabayashi N, MacDonald TY, Ghandi M, et al. 2013. Punctuated evolution of prostate cancer genomes. *Cell* **153:** 666–677.

Barbieri CE, Baca SC, Lawrence MS, Demichelis F, Blattner M, Theurillat J-P, White TA, Stojanov P, Van Allen E, Stransky N, et al. 2012. Exome sequencing identifies recurrent *SPOP*, *FOXA1* and *MED12* mutations in prostate cancer. *Nat Genet* **44:** 685–689.

Bass AJ, Lawrence MS, Brace LE, Ramos AH, Drier Y, Cibulskis K, Sougnez C, Voet D, Saksena G, Sivachenko A, et al. 2011. Genomic sequencing of colorectal adenocarcinomas identifies a recurrent *VTI1A-TCF7L2* fusion. *Nat Genet* **43:** 964–968.

Beà S, Valdés-Mas R, Navarro A, Salaverria I, Martín-Garcia D, Jares P, Giné E, Pinyol M, Royo C, Nadeu F, et al. 2013. Landscape of somatic mutations and clonal evolution in mantle cell lymphoma. *Proc Natl Acad Sci* **110:** 18250–18255.

Berger MF, Lawrence MS, Demichelis F, Drier Y, Cibulskis K, Sivachenko AY, Sboner A, Esgueva R, Pflueger D, Sougnez C, et al. 2011. The genomic complexity of primary human prostate cancer. *Nature* **470:** 214–220.

Berger MF, Hodis E, Heffernan TP, Deribe YL, Lawrence MS, Protopopov A, Ivanova E, Watson IR, Nickerson E, Ghosh P, et al. 2012. Melanoma genome sequencing reveals frequent *PREX2* mutations. *Nature* **485:** 502–506.

Brastianos PK, Horowitz PM, Santagata S, Jones RT, McKenna A, Getz G, Ligon KL, Palescandolo E, Van Hummelen P, Ducar MD, et al. 2013. Genomic sequencing of meningiomas identifies oncogenic *SMO* and *AKT1* mutations. *Nat Genet* **45:** 285–289.

Brennan CW, Verhaak RGW, McKenna A, Campos B, Noushmehr H, Salama SR, Zheng S, Chakravarty D, Sanborn JZ, Berman SH, et al. 2013. The somatic genomic landscape of glioblastoma. *Cell* **155:** 462–477.

Bruin EC, de McGranahan N, Mitter R, Salm M, Wedge DC, Yates L, Jamal-Hanjani M, Shafi S, Murugaesu N, Rowan AJ, et al. 2014. Spatial and temporal diversity in genomic instability processes defines lung cancer evolution. *Science* **346:** 251–256.

Carreira S, Romanel A, Goodall J, Grist E, Ferraldeschi R, Miranda S, Prandi D, Lorente D, Frenel J-S, Pezaro C, et al. 2014. Tumor clone dynamics in lethal prostate cancer. *Sci Transl Med* **6:** 254ra125.

Chapman MA, Lawrence MS, Keats JJ, Cibulskis K, Sougnez C, Schinzel AC, Harview CL, Brunet J-P, Ahmann GJ, Adli M, et al. 2011. Initial genome sequencing and analysis of multiple myeloma. *Nature* **471:** 467–472.

Chen X, Bahrami A, Pappo A, Easton J, Dalton J, Hedlund E, Ellison D, Shurtleff S, Wu G, Wei L, et al. 2014. Recurrent somatic structural variations contribute to tumorigenesis in pediatric osteosarcoma. *Cell Rep* **7:** 104–112.

Chen L, Shern JF, Wei JS, Yohe ME, Song YK, Hurd L, Liao H, Catchpoole D, Skapek SX, Barr FG, et al. 2015. Clonality and evolutionary history of rhabdomyosarcoma. *PLoS Genet* **11:** e1005075.

Cooper CS, Eeles R, Wedge DC, Van Loo P, Gundem G, Alexandrov LB, Kremeyer B, Butler A, Lynch AG, Camacho N, et al. 2015. Analysis of the genetic phylogeny of multifocal prostate cancer identifies multiple independent clonal expansions in neoplastic and morphologically normal prostate tissue. *Nat Genet* **47:** 367–372.

Dieci MV, Arnedos M, Andre F, Soria JC. 2013. Fibroblast growth factor receptor inhibitors as a cancer treatment: from a biologic rationale to medical perspectives. *Cancer Discov* **3:** 264–279.

Ding L, Ellis MJ, Li S, Larson DE, Chen K, Wallis JW, Harris CC, McLellan MD, Fulton RS, Fulton LL, et al. 2010. Genome remodelling in a basal-like breast cancer metastasis and xenograft. *Nature* **464:** 999–1005.

Ding L, Kim M, Kanchi KL, Dees ND, Lu C, Griffith M, Fenstermacher D, Sung H, Miller CA, Goetz B, et al. 2014. Clonal architectures and driver mutations in metastatic melanomas. *PLoS One* **9:** e111153.

Dulak AM, Stojanov P, Peng S, Lawrence MS, Fox C, Stewart C, Bandla S, Imamura Y, Schumacher SE, Shefler E, et al. 2013. Exome and whole-genome sequencing of esophageal adenocarcinoma identifies recurrent driver events and mutational complexity. *Nat Genet* **45:** 478–486.

Egan JB, Shi C-X, Tembe W, Christoforides A, Kurdoglu A, Sinari S, Middha S, Asmann Y, Schmidt J, Braggio E, et al. 2012. Whole-genome sequencing of multiple myeloma from diagnosis to plasma cell leukemia reveals genomic initiating events, evolution, and clonal tides. *Blood* **120:** 1060–1066.

Ellis MJ, Ding L, Shen D, Luo J, Suman VJ, Wallis JW, Van Tine BA, Hoog J, Goiffon RJ, Goldstein TC, et al. 2012. Whole-genome analysis informs breast cancer response to aromatase inhibition. *Nature* **486:** 353–360.

Engle EK, Fisher DAC, Miller CA, McLellan MD, Fulton RS, Moore DM, Wilson RK, Ley TJ, Oh ST. 2015. Clonal evolution revealed by whole genome sequencing in a case of primary myelofibrosis transformed to secondary acute myeloid leukemia. *Leukemia* **29:** 869–876.

Govindan R, Ding L, Griffith M, Subramanian J, Dees ND, Kanchi KL, Maher CA, Fulton R, Fulton L, Wallis J, et al. 2012. Genomic landscape of non–small cell lung cancer in smokers and never-smokers. *Cell* **150:** 1121–1134.

Griffith M, Griffith OL, Coffman AC, Weible JV, McMichael JF, Spies NC, Koval J, Das I, Callaway MB, Eldred JM, et al. 2013. DGIdb: mining the druggable genome. *Nat Methods* **10:** 1209–1210.

Gundem G, Van Loo P, Kremeyer B, Alexandrov LB, Tubio JMC, Papaemmanuil E, Brewer DS, Kallio HML, Högnäs G, Annala M, et al. 2015. The evolutionary history of lethal metastatic prostate cancer. *Nature* **520:** 353–357.

Haffner MC, Mosbruger T, Esopi DM, Fedor H, Heaphy CM, Walker DA, Adejola N, Gürel M, Hicks J, Meeker AK, et al. 2013. Tracking the clonal origin of lethal prostate cancer. *J Clin Invest* **123:** 4918–4922.

Haffner MC, Marzo AMD, Yegnasubramanian S, Epstein JI, Carter HB. 2015. Diagnostic challenges of clonal heterogeneity in prostate cancer. *J Clin Oncol* **33:** e38–e40.

Ho AS, Kannan K, Roy DM, Morris LGT, Ganly I, Katabi N, Ramaswami D, Walsh LA, Eng S, Huse JT, et al. 2013. The mutational landscape of adenoid cystic carcinoma. *Nat Genet* **45:** 791–798.

Hong MKH, Macintyre G, Wedge DC, Van Loo P, Patel K, Lunke S, Alexandrov LB, Sloggett C, Cmero M, Marass F, et al. 2015. Tracking the origins and drivers of subclonal metastatic expansion in prostate cancer. *Nat Commun* **6:** 6605.

Imielinski M, Berger AH, Hammerman PS, Hernandez B, Pugh TJ, Hodis E, Cho J, Suh J, Capelletti M, Sivachenko A, et al. 2012. Mapping the hallmarks of lung adenocarcinoma with massively parallel sequencing. *Cell* **150:** 1107–1120.

Kan Z, Zheng H, Liu X, Li S, Barber TD, Gong Z, Gao H, Hao K, Willard MD, Xu J, et al. 2013. Whole-genome sequencing identifies recurrent mutations in hepatocellular carcinoma. *Genome Res* **23:** 1422–1433.

Kim H, Zheng S, Amini SS, Virk SM, Mikkelsen T, Brat DJ, Grimsby J, Sougnez C, Muller F, Hu J, et al. 2015. Whole-genome and multisector exome sequencing of primary and post-treatment glioblastoma reveals patterns of tumor evolution. *Genome Res* **25:** 316–327.

Kovac M, Navas C, Horswell S, Salm M, Bardella C, Rowan A, Stares M, Castro-Giner F, Fisher R, de Bruin EC, et al. 2015. Recurrent chromosomal gains and heterogeneous driver mutations characterise papillary renal cancer evolution. *Nat Commun* **6:** 6336.

Langmead B, Salzberg SL. 2012. Fast gapped-read alignment with Bowtie 2. *Nat Methods* **9:** 357–359.

Lindberg J, Kristiansen A, Wiklund P, Grönberg H, Egevad L. 2015. Tracking the origin of metastatic prostate cancer. *Eur Urol* **67:** 819–822.

Morin RD, Mungall K, Pleasance E, Mungall AJ, Goya R, Huff RD, Scott DW, Ding J, Roth A, Chiu R, et al. 2013. Mutational and structural analysis of diffuse large B-cell lymphoma using whole-genome sequencing. *Blood* **122:** 1256–1265.

Morrison CD, Liu P, Woloszynska-Read A, Zhang J, Luo W, Qin M, Bshara W, Conroy JM, Sabatini L, Vedell P, et al. 2014. Whole-genome sequencing identifies genomic heterogeneity at a nucleotide and chromosomal level in bladder cancer. *Proc Natl Acad Sci* **111:** E672–E681.

Nadauld LD, Garcia S, Natsoulis G, Bell JM, Miotke L, Hopmans ES, Xu H, Pai RK, Palm C, Regan JF, et al. 2014. Metastatic tumor evolution and organoid modeling implicate *TGFBR2* as a cancer driver in diffuse gastric cancer. *Genome Biol* **15:** 428.

Newburger DE, Kashef-Haghighi D, Weng Z, Salari R, Sweeney RT, Brunner AL, Zhu SX, Guo X, Varma S, Troxell ML, et al. 2013. Genome evolution during progression to breast cancer. *Genome Res* **23:** 1097–1108.

Nik-Zainal S, Van Loo P, Wedge DC, Alexandrov LB, Greenman CD, Lau KW, Raine K, Jones D, Marshall J, Ramakrishna M, et al. 2012. The life history of 21 breast cancers. *Cell* **149:** 994–1007.

Ouyang L, Lee J, Park C-K, Mao M, Shi Y, Gong Z, Zheng H, Li Y, Zhao Y, Wang G, et al. 2014. Whole-genome sequencing of matched primary and metastatic hepatocellular carcinomas. *BMC Med Genomics* **7:** 2.

Palmberg C, Koivisto P, Kakkola L, Tammela TL, Kallioniemi OP, Visakorpi T. 2000. Androgen receptor gene amplification at primary progression predicts response to combined androgen blockade as second line therapy for advanced prostate cancer. *J Urol* **164:** 1992–1995.

Patch A-M, Christie EL, Etemadmoghadam D, Garsed DW, George J, Fereday S, Nones K, Cowin P, Alsop K, Bailey PJ. 2015. Whole-genome characterization of chemoresistant ovarian cancer. *Nature* **521:** 489–494.

Pugh TJ, Morozova O, Attiyeh EF, Asgharzadeh S, Wei JS, Auclair D, Carter SL, Cibulskis K, Hanna M, Kiezun A, et al. 2013. The genetic landscape of high-risk neuroblastoma. *Nat Genet* **45:** 279–284.

Quinlan AR, Hall IM. 2010. BEDTools: a flexible suite of utilities for comparing genomic features. *Bioinforma Oxf Engl* **26:** 841–842.

Robinson D, Van Allen EM, Wu Y-M, Schultz N, Lonigro RJ, Mosquera J-M, Montgomery B, Taplin M-E, Pritchard CC, Attard G, et al. 2015. Integrative clinical genomics of advanced prostate cancer. *Cell* **161:** 1215–1228.

Roychowdhury S, Iyer MK, Robinson DR, Lonigro RJ, Wu Y-M, Cao X, Kalyana-Sundaram S, Sam L, Balbin OA, Quist MJ, et al. 2011. Personalized oncology through integrative high-throughput sequencing: a pilot study. *Sci Transl Med* **3:** 111ra121.

The 1000 Genomes Project Consortium. 2015. A global reference for human genetic variation. *Nature* **526:** 68–74.

Turajlic S, Furney SJ, Lambros MB, Mitsopoulos C, Kozarewa I, Geyer FC, MacKay A, Hakas J, Zvelebil M, Lord CJ, et al. 2012. Whole genome sequencing of matched primary and metastatic acral melanomas. *Genome Res* **22:** 196–207.

Walter MJ, Shen D, Ding L, Shao J, Koboldt DC, Chen K, Larson DE, McLellan MD, Dooling D, Abbott R, et al. 2012. Clonal architecture of secondary acute myeloid leukemia. *N Engl J Med* **366:** 1090–1098.

Wang K, Li M, Hakonarson H. 2010. ANNOVAR: functional annotation of genetic variants from high-through-put sequencing data. *Nucleic Acids Res* **38:** e164.

Wang K, Yuen ST, Xu J, Lee SP, Yan HHN, Shi ST, Siu HC, Deng S, Chu KM, Law S, et al. 2014. Whole-genome sequencing and comprehensive molecular profiling identify new driver mutations in gastric cancer. *Nat Genet* **46:** 573–582.

Welch JS, Ley TJ, Link DC, Miller CA, Larson DE, Koboldt DC, Wartman LD, Lamprecht TL, Liu F, Xia J, et al. 2012. The origin and evolution of mutations in acute myeloid leukemia. *Cell* **150:** 264–278.

Yates LR, Gerstung M, Knappskog S, Desmedt C, Gundem G, Van Loo P, Aas T, Alexandrov LB, Larsimont D, Davies H, et al. 2015. Subclonal diversification of primary breast cancer revealed by multiregion sequencing. *Nat Med* **21:** 751–759.

Zhang J, Grubor V, Love CL, Banerjee A, Richards KL, Mieczkowski PA, Dunphy C, Choi W, Au WY, Srivastava G, et al. 2013. Genetic heterogeneity of diffuse large B-cell lymphoma. *Proc Natl Acad Sci* **110:** 1398–1403.

Zhao X-Y, Malloy PJ, Krishnan AV, Swami S, Navone NM, Peehl DM, Feldman D. 2000. Glucocorticoids can promote androgen-independent growth of prostate cancer cells through a mutated androgen receptor. *Nat Med* **6:** 703–706.